INTERNATIONAL JOURNAL FOR NUMERICAL METHODS IN FLUIDS, VOL. 5, 601–614 (1985)

ON THE PERFORMANCE OF QUADRILATERAL FINITE ELEMENTS IN THE SOLUTION TO THE STOKES EQUATIONS IN PERIODIC STRUCTURES

A. E. SÁEZ AND R. G. CARBONELL

Department of Chemical Engineering, North Carolina State University, Raleigh, North Carolina 27695–7905, U.S.A.

SUMMARY

The use of the finite element method in solving the problem of flow of a Newtonian fluid in periodically constricted tubes is explored. The performance of eight node serendipity and nine node Lagrangian elements is compared. It was found that the Lagrangian element results in unstable velocity fields when stagnant or recirculation regions are present. This is characteristic of tubes with large expansion zones. The eight node element does not exhibit instabilities. Both elements give accurate pressure fields. This behaviour is contrary to traditional results obtained for flow problems with similar geometrical characteristics. This suggests that the periodicity of the boundary conditions might be the cause of the instabilities in the numerical solution.

The use of the continuity equation to simplify the viscous terms in the Stokes equations resulted, in this particular case, in a deterioration of the rate of convergence of the algorithm.

KEY WORDS Finite Elements Stokes Equations Periodically Constricted Tubes Quadrilateral Elements

INTRODUCTION

In recent times there has been an increasing trend to use the finite element method in the solution of fluid mechanics and transport phenomena problems. This technique has proved to be very adequate for treating irregular and complicated geometries owing to the versatility of the method in the description of the boundaries of the solution domain. Furthermore, complex boundary conditions can be easily incorporated into the numerical solution in the form of boundary integrals, which are specially useful for treating natural boundary conditions.

Early attempts to solve the Navier–Stokes equations in closed domains via finite elements were performed by Atkinson *et al.*[1], Oden and Wellford[2] and Taylor and Hood.[3] These first investigations focused mainly on the efficiency of the various finite element formulations of the flow problem. Taylor and Hood[3] concluded that the primitive variables (pressure–velocity) formulation of the Navier–Stokes equations provided a finite element algorithm more efficient from a computational point of view than that obtained from a streamline–vorticity formulation. These investigators also determined that the finite element algorithm was better when the basis functions used to represent the velocity were an order higher than those used to represent the pressure. This scheme is called mixed interpolation and its advantages have been further studied by Olson and Tuann[4] and more recently by Sani *et al.*[5,6]

The choice of the type of finite element to use in the solution of a particular problem has been traditionally based on experience or trial and error. Recently, more effort has been devoted to comparing the performance of various elements and approximating functions. Huyakorn

0271–2091/85/070601–14$01.40

Received 10 October 1984
Revised 7 January 1985

et al.[7] compaired the solutions obtained by using several elements for two test problems involving steady flow through a sudden expansion and free thermal convection in a square cavity. The unstable pressure patterns observed when the Navier–Stokes equations are solved by using certain types of finite elements were studied in detail by Sani *et al.*[5,6]

One of the objectives of this work is to compare the performance of two types of quadrilateral elements (the 8-node serendipity and the 9-node Lagrangian elements) in the solution to the Stokes and continuity equations for the case of steady flow through periodically constricted tubes. This problem has been previously solved by collocation methods,[8,9] finite differences[10] and perturbation techniques.[11] The solution is of interest not only to the study of transport phenomena in constricted tubes but also as an important step in the modelling of porous media processes.[8,9,12]

FORMULATION OF THE PROBLEM

Consider the viscous flow of an incompressible Newtonian fluid through a periodically constricted tube consisting of the repetition along the x-axis of the unit cell structure shown in Figure 1, under steady-state conditions. The periodicity of the wall profile can be expressed as

$$r'_\sigma(x') = r'_\sigma(x' \pm nl), \quad n = 0, 1, \ldots \tag{1}$$

The continuity and momentum equations are

$$\nabla' \cdot \mathbf{v}' = 0, \tag{2}$$

$$0 = -\nabla' P' + \rho \mathbf{g} + \nabla' \cdot \boldsymbol{\tau}', \tag{3}$$

where the primes denote dimensional quantities. The stress tensor is given by

$$\boldsymbol{\tau} = \mu[\nabla' \mathbf{v}' + (\nabla' \mathbf{v}')^{\mathrm{T}}]. \tag{4}$$

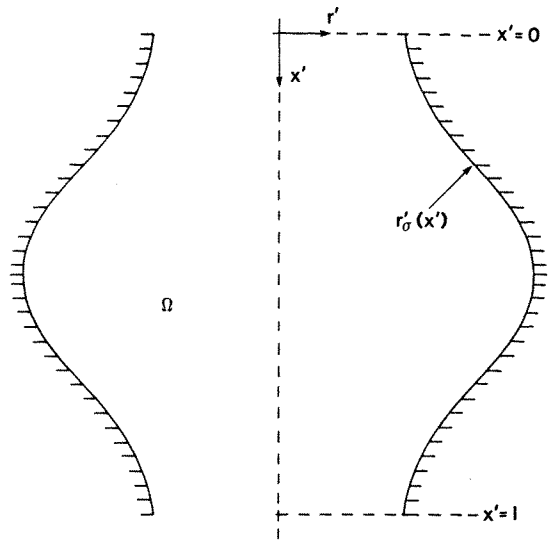

Figure 1. Periodically constricted tube. Unit cell

The boundary conditions are

1. No-slip at the wall:

$$\mathbf{v}' = 0, \quad \text{at } r' = r'_\sigma. \tag{5}$$

2. Symmetry about $r' = 0$:

$$\frac{\partial \mathbf{v}'}{\partial r'} = 0, \quad \text{at } r' = 0. \tag{6}$$

3. Spatial periodicity of the surface (equation (1)).

The set of equations and boundary conditions stated above is invariant to a co-ordinate transformation of the form

$$x' \xrightarrow{T(x')} x' \pm nl, \quad n = 0, 1, \ldots$$

Therefore, the solution to the set of equations can be proved to exhibit spatial periodicity, i.e. $\mathbf{v}'$ and $\nabla P'$ are spatially periodic. The fact that the gradient of the pressure field is spatially periodic means that the pressure can be decomposed into the sum of a periodic contribution and a linear term as follows (for details see Reference 13):

$$P' = P'_* + \frac{\Delta \bar{P} x'}{l}, \tag{7}$$

where P'_* is periodic and $\Delta \bar{P}$ is the area averaged pressure drop through the unit cell,

$$\Delta \bar{P} = \bar{P}(x' + l) - \bar{P}(x'). \tag{8}$$

The area-averaged pressure is defined as

$$\bar{P}(x') = \frac{1}{A_T} \int_{A_T} P' \mathrm{d}A, \tag{9}$$

where $A_T(x')$ is the local cross-sectional area of the tube.

Substituting equation (7) into equation (3) yields

$$0 = -\nabla' P'_* - \frac{\Delta \mathscr{P}'}{l} \mathbf{e}_x + \nabla' \cdot \boldsymbol{\tau}', \tag{10}$$

where $\mathbf{e}_x$ is a unit vector in the x-direction and $\Delta P'/l$ is the pressure drop including hydrostatic contributions, defined by

$$\frac{\Delta \mathscr{P}'}{l} = \frac{\Delta \bar{P}}{l} - \rho g. \tag{11}$$

The statement of the problem can be reduced to its simplest form by choosing the following set of dimensionless variables:

$$x = x'/l, \tag{12}$$

$$r = r'/l, \tag{13}$$

$$P_* = P'_*/(-\Delta \mathscr{P}'), \tag{14}$$

$$\mathbf{v} = \mu \mathbf{v}'/(-l \Delta \mathscr{P}'). \tag{15}$$

The basic equations in dimensionless form are

$$\nabla \cdot \mathbf{v} = 0, \tag{16}$$

$$0 = -\nabla P_* + \nabla \cdot \boldsymbol{\tau} + \mathbf{e}_x, \tag{17}$$

$$\boldsymbol{\tau} = \nabla \mathbf{v} + (\nabla \mathbf{v})^{\mathrm{T}}. \tag{18}$$

With boundary conditions

$$\mathbf{v} = 0, \quad \text{at} \quad r = r_\sigma(x), \tag{19}$$

$$\frac{\partial \mathbf{v}}{\partial r} = 0, \quad \text{at} \quad r = 0, \tag{20}$$

$$\mathbf{v}(x) = \mathbf{v}(x \pm n), \tag{21}$$

$$P_*(x) = P_*(x \pm n). \tag{22}$$

It can be easily proved that this problem has a unique solution for the velocity field and a unique solution for the periodic part of the pressure field up to an arbitrary constant.[13] Furthermore, the basic equations show that the solutions for $\mathbf{v}$ and P_* are only functions of the geometry of the unit cell, namely $r_\sigma(x)$. Therefore, for a given geometry, the solution to equations (16) to (22) provides all the information required to characterize the flow of a viscous fluid for any value of the density, the viscosity and the average pressure drop. Notice that a knowledge of $\mathbf{v}(x, r)$ allows one to find, through equation (15), the proportionality relation between the macroscopic pressure drop $(\Delta \mathscr{P}'/l)$ and the flow rate.

FINITE ELEMENT DISCRETIZATION

The system of equations (16)–(22) was solved by means of the Galerkin finite element method. The integration domain (Ω) is subdivided into M quadrilateral, straight-sided elements $(\Omega_m, m = 1, 2, \ldots, M)$. The velocity and pressure fields are approximated as follows:

$$\hat{\mathbf{v}} = \sum_{i=1}^{N} \varphi_i \hat{\mathbf{v}}_i, \tag{23}$$

$$\hat{P}_* = \sum_{\substack{i=1 \\ (i=i_p)}}^{N} \psi_i \hat{P}_{*i}, \tag{24}$$

where φ_i is a second-order approximating function and ψ_i a first-order one, providing a mixed interpolation scheme. The circumflex in these equations represents approximate values, so that $\hat{\mathbf{v}}_i$ and $\hat{P}_{*i}$ are the approximate values of velocity and periodic pressure at node i. The quantity N represents the total number of nodes in the system. Notice that $\hat{\mathbf{v}}_i$ exists for all nodes i whereas $\hat{P}_{*i}$ exists only for those nodes $i = i_p$ where a pressure approximation is defined. Fewer nodes are required in the approximation of P_* owing to the nature of the mixed interpolation scheme.

The mixed interpolation scheme chosen is particularly of two types of quadrilateral elements commonly used: the eight-node serendipity element and the nine-node Lagrangian element. Both elements result in a biquadratic approximation for the velocity field and a bilinear approximation for the pressure field. The fact that the pressure approximation is linear implies that there are four nodes defining pressure approximations in one element, whereas the velocity is defined in all the nodes (either eight or nine). The shape functions φ_i and ψ_i for both types of elements,

along with some details regarding the structure of the approximations that they represent, can be found elsewhere.[13,14]

The application of the Galerkin technique to the basic equations, along with the use of the approximations (23) and (24), leads to the following discretization of the problem.[13]

Equation (16) leads to the continuity equation weighted residual statement:

$$R_{ci} = \sum_{m=1}^{M} \sum_{j=1}^{N} \int_{\Omega_m} \psi_i \nabla \cdot (\hat{\mathbf{v}}_j \varphi_j) \mathrm{d}V, \tag{25}$$

valid for all nodes i except $i = i_\pi$, where i_π is an arbitrary node at which a datum level is set for the P_* field (see below).

Equations (17) and (18) lead to the momentum equation weighted residual statement

$$\mathbf{R}_{vi} = \sum_{m=1}^{M} \left\{ - \sum_{j=1}^{N} \hat{P}_{*j} \int_{\Omega_m} \nabla \psi_j \varphi_i \mathrm{d}V + \mathbf{e}_x \int_{\Omega_m} \varphi_i \mathrm{d}V - \sum_{j=1}^{N} \int_{\Omega_m} (\nabla \phi_i \cdot \hat{\mathbf{v}}_j \nabla \phi_j + \nabla \varphi_i \cdot \nabla \hat{\mathbf{v}}_j \varphi_j) \right\} \mathrm{d}V, \tag{26}$$

valid for all nodes i except $i = i_s$, where i_s denotes all nodes at the solid surface at which the no-slip condition is applied. This condition (equation (19)) is implemented in the form of admissibility constraints,

$$\hat{\mathbf{v}}_i = 0, \tag{27}$$

valid for nodes $i = i_s$.

Finally, the complete determination of P_* requires a datum level, which is obtained by substituting the continuity equation weighted residual at an arbitrary node by the admissibility condition

$$\hat{P}_{*i} = 0, \tag{28}$$

valid at a node $i = i_\pi$. The location of node i_π in the finite element mesh had no appreciable effect in the solution except for very coarse grids. For convenience in the implementation of the computer program, i_π was located at the solid surface.

Equations (25) and (26) equated to zero plus equations (27) and (28) represent a complete linear system of algebraic equations. Notice that boundary conditions (20)–(22) do not appear explicitly in the final formulation. Condition (20) is a natural boundary condition that is used in the development of equation (26). The periodicity conditions (equations (21) and (22)) are, as we have discussed, a consequence of the translational symmetry of the domain of integration. This translational symmetry can be conceptualized as a condition imposed on the integration domain rather than on the dependent variables. Consider the periodic domain shown in Figure 2. According to our formulation, the dependent variables $\mathbf{v}$ and P_* have the same functional form at two arbitrary lines AB and A′B′ separated by the unit cell length. Since the equations are not affected by the displacement of the x-axis over that distance, line AB can be conceptualized as being the same line A′B′. In other words, nodes i_k and i_{k+1} are mathematically equivalent, namely the equations for node i_k will have contributions from elements m_k and m_{k+1}. This is the same as saying that the domain is 'closed' so that lines AB and A′B′ coincide and, therefore, are not external boundaries of the domain. The closure of the domain through the periodicity boundary pre-empts the periodicity conditions. We followed this scheme in the numerical calculations since it simplified the formulation (essentially, the equivalence of the nodes at the boundaries eliminates one line of nodes).

The absence of inertial terms in the momentum equations allows a simplification of the problem. If the unit cell is chosen so that the wall profile is symmetric about $x = 0{\cdot}5$, as in

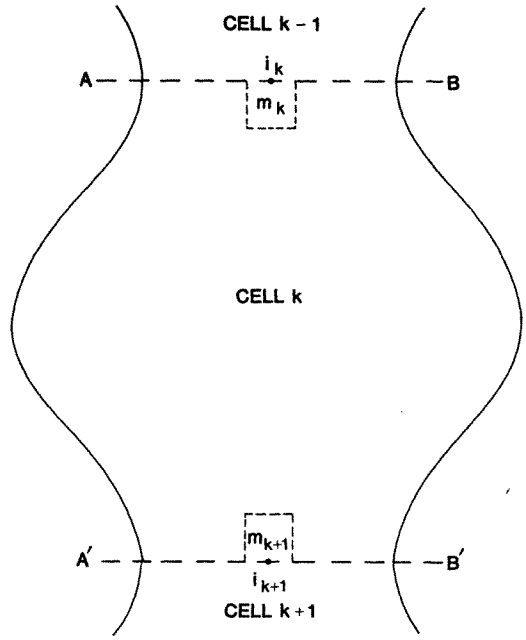

Figure 2. Periodicity and the integration domain

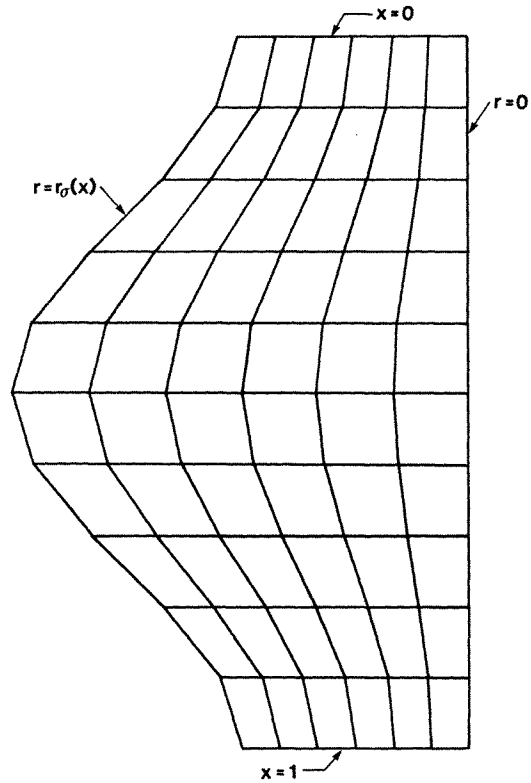

Figure 3. Finite element grid

Figure 1, then it can be easily shown[13] that the axial component of the velocity is also symmetric whereas the radial component of the velocity and the periodic pressure are skew-symmetric about $x = 0{\cdot}5$. This fact allows a solution to the problem in half the unit cell, considerably reducing the computational effort.

The finite element grids were generated by means of the isoparametric scheme presented by Herrmann.[15] A typical grid arrangement is shown in Figure 3. The centre nodes in the nine-node element grids are located according to the following equations:

$$r_* = \frac{1}{2}\sum_{i=1}^{4} r_{ci} - \frac{1}{4}\sum_{i=1}^{4} r_{mi},$$

$$x_* = \frac{1}{2}\sum_{i=1}^{4} x_{ci} - \frac{1}{4}\sum_{j=1}^{4} x_{mi},$$

where the subscripts $*$, c and m denote centre, corner and mid-side nodes, respectively.

The integral terms in equations (25) and (26) were evaluated by means of 2×2 Gaussian quadrature. The use of straight-sided, distorted elements (see Figure 3) and a biquadratic approximation for the velocity fields implies that integrals with high order integrands are not evaluated exactly by 2×2 quadrature, as shown by Leone *et al.*[16] However, the overall error of the biquadratic approximation is of order two[17] and the scheme used guarantees that integrals of second order terms are exact. Therefore, the error introduced by the 2×2 scheme is lower than the intrinsic error of the finite element formulation. Once the coefficients in equations (25) and (26) were evaluated, the resulting system of equations was solved by means of a frontal solver procedure, very similar to that described by Hood.[18]

RESULTS

A computer program was developed to solve the problem stated in the previous sections. The program was written in FORTRAN and run on a PDP-11 computer. Detailed results of the performance of the program as well as solutions for several wall geometries are reported by Sáez.[13] In this paper we will present some results regarding the effect of the formulation of the momentum equation on the rate of convergence of the algorithm. We will also analyse the performance of eight- and nine-node elements.

Effect of the formulation of the viscous terms on algorithm performance

The viscous flow equations of motion (equation (17)) can be formulated in two equivalent ways, one having $\nabla^2\mathbf{v}$ as the viscous term and the other having $\nabla\cdot\boldsymbol{\tau}$. The latter was used in the previous sections. The two formulations are mathematically equivalent, since

$$\nabla\cdot\boldsymbol{\tau} = \nabla^2\mathbf{v} + \nabla\cdot(\nabla\mathbf{v})^{\mathrm{T}},$$

and

$$\nabla\cdot(\nabla\mathbf{v})^{\mathrm{T}} = 0$$

because of continuity (equation (16)). However, the weighted residual statement is somewhat different in the two cases. If $\nabla^2\mathbf{v}$ is used as the viscous term in the original equation, then the term $\nabla\varphi_i\cdot\hat{\mathbf{v}}_j\nabla\varphi_j$ is not present in the last integral of equation (26). The fact that the two formulations are mathematically equivalent implies that they will converge to the same solution as the finite element grid is made finer. This does not mean that the results will be the same for coarse grids, so that the convergence behaviours of the two schemes can be different. Indeed,

the scheme that considers the viscous terms in the form $\nabla \cdot \tau$ has a faster rate of convergence. To illustrate this point, let us consider the solution to the flow problem in a sinusoidal tube with the following wall profile:

$$r_o(x) = 0{\cdot}1(1 - 0{\cdot}333 \cos 2\pi x). \tag{29}$$

Figure 4 shows a comparison between the two schemes. In this Figure M_x represents the number of elements of the grid in the x-direction. The calculations were performed with 6 elements in the r-direction ($M_r = 6$). Notice that $M = M_r M_x$. We have used as the parameter defining convergence the ratio Q_m/Q_M, where Q_m represents the minimum value of the flow rate as a function of x and Q_M the maximum. For coarse grids the maximum flow rate, Q_M, occurs at the constriction region whereas the minimum flow rate, Q_m, occurs at the expansion region. As the grid becomes finer and the solution approaches the exact solution, the flow rate becomes independent of x and Q_m/Q_M becomes equal to one. The results plotted in Figure 4 ($M_r = 6$) coincide with those obtained with $M_r = 5$ and 4 so that convergence in terms of M_r has been achieved. The difference between the two schemes is not large but it is certainly measurable (see Figure 4). These results show that the formulation of the equations of motion in terms of the gradient of the stress tensor ($\nabla \cdot \tau$) yields a computationally more efficient finite element algorithm.

The ratio of flow rates, Q_m/Q_M, is a strict measure of convergence since it is affected not only by the intrinsic error in the finite element computations, but also by the error involved in the calculation of the flow rates through numerical integration. We found that a flow rate ratio of 0·9 was enough to get velocity and pressure profiles practically indistinguishable from the exact solution.

Effect of element choice of algorithm performance

The problem under consideration in the present work was solved by using two types of finite elements: the eight-node serendipity element and the nine-node Lagrangian element. As we

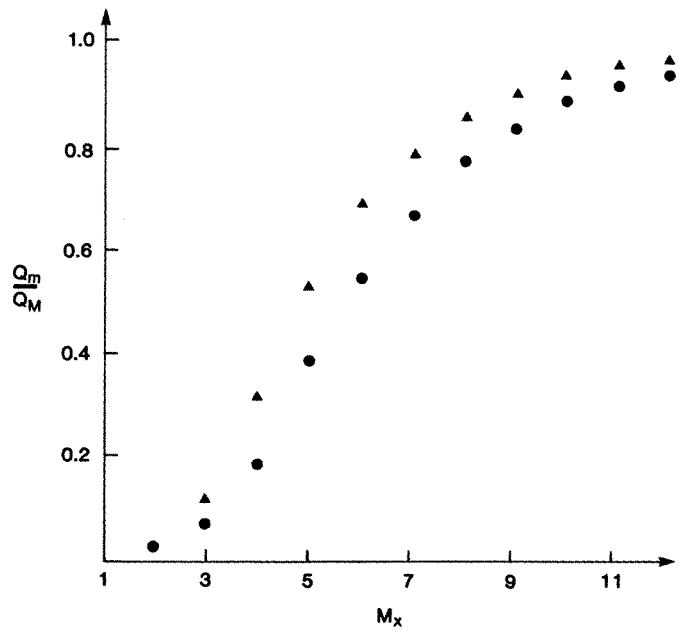

Figure 4. Effect of the formulation of the viscous terms on the rate of convergence: ●, $\nabla^2 v$ scheme; ▲, $\nabla \cdot \tau$ scheme

mentioned before, the total number of nodes in those elements corresponds to the nodes at which an approximate velocity is defined. The geometry of the element, as well as the pressure approximation, is linear so that it is defined by four nodes only. The Lagrangian elements are constructed by taking the product of one-dimensional Lagrange polynomials in both directions (r and x), these polynomials being of the same order. For the case of bi-quadratic approximations, the number of coefficients is nine. Thus, if we approximate any function f in the r–x plane by means of Lagrangian second-order elements, the interpolating function, $\hat{f}$, would be given by

$$\hat{f}^{(9)}(r, x) = a + br + cx + dr^2 + ex^2 + grx + hrx^2 + jxr^2 + kx^2r^2.$$

On the other hand, the eight-node serendipity element is constructed by taking the product of a Lagrange interpolating polynomial of second order with a first-order polynomial. Hence, the eight-node element leads to an approximation of the form

$$\hat{f}^{(8)}(r, x) = a' + b'r + c'x + d'r^2 + e'x^2 + g'rx + h'rx^2 + j'xr^2.$$

The only structural difference between the two approximations is the fourth order term x^2r^2. As pointed out by Taylor,[19] both schemes provide a complete set of functions for second-order approximations. Furthermore,[17] the error is of the same order of magnitude, since terms of global order 3 or 4 do not contribute to the error bounds. Hence, the two schemes should have similar performances in terms of global accuracy.

The fact that the nine-node element introduces an extra variable indicates that the eight-node element should be more efficient from a computational point of view. As a matter of fact, this idea led to the formulation of elements of the serendipity type by Zienkiewicz *et al.*[20] However, the extra variable, represented by the centre node, can be appropriately removed from the formulation by means of algebraic manipulation of the equations. The resulting system of equations has a similar structure for both elements in that the only difference lies on the coefficients of the element matrices. Therefore, the computational effort is similar for both elements.

It has been observed in previous investigations that the two elements under consideration have in some cases different performances. For instance, Huyakorn *et al.*[7] concluded that the eight-node element was ostensibly less accurate that the nine-node element after using both of them in two test problems. The inaccuracies exhibited by the solution employing eight-node elements were basically the presence of an oscillatory behaviour of the approximate pressure fields. One of the test problems solved by Huvakorn *et al.* is very similar to the one considered in this work. These investigators solved the Navier–Stokes equations corresponding to steady flow through a sudden expansion. This problem differs from the flow through periodically constricted tubes mainly in the boundary conditions. Huyakorn *et al.* imposed a parabolic, Poiseuille flow boundary condition at the entrance of the system (constriction) whereas at the exit (expansion) they considered that the normal stress was equal to zero. As we discussed before, the periodicity of the geometry in the periodically constricted tube implies that the boundary conditions for the velocity and the periodic part of the pressure field at entrances and exits can be transformed to a constraint imposed on the integration domain.

We obtained two types of results when eight- and nine-node elements were used to solve the problem under consideration, depending on the geometry of the unit cell. To illustrate these results, let us consider a sinusoidal wall geometry. For low to moderate values of the amplitude of the wall oscillations, both elements give indistinguishable results in terms of velocity and pressure fields for all grid sizes. For example, for the wall profile given by equation (29), Figures 5–7 show axial velocity profiles and periodic pressure profiles obtained by using a grid of 60 elements. The dots correspond to the results of using nine-node elements and the solid line is a smooth line drawn through the points resulting from using eight-node elements. The solution

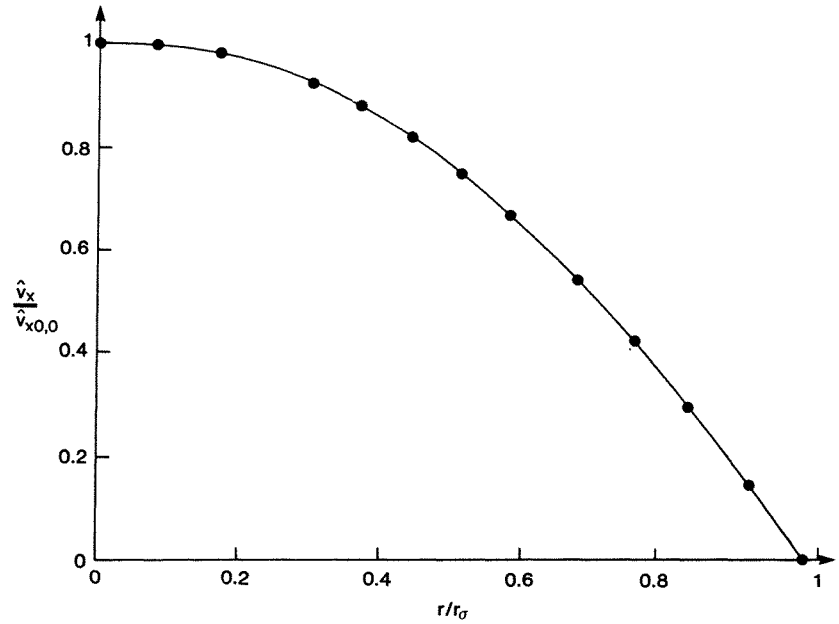

Figure 5. Axial velocity at $x = 0$. Wall profile described by equation (29)

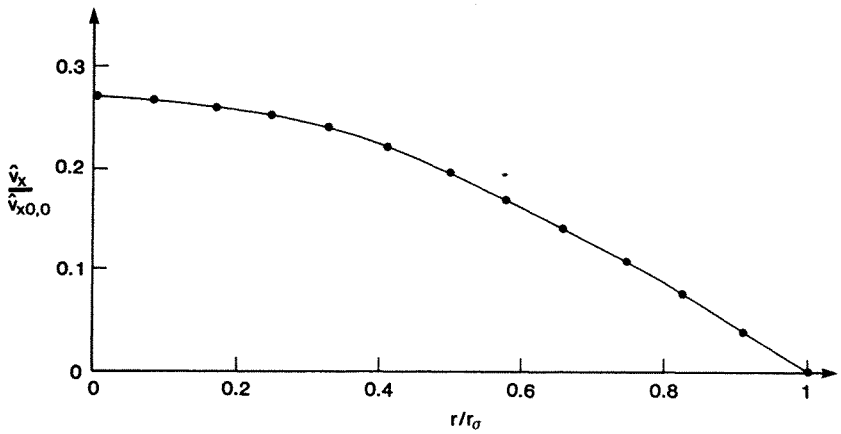

Figure 6. Axial velocity at $x = 0{\cdot}5$. Wall profile described by equation (29)

presented in Figure 5–7 coincides with those reported by Fedkiw and Newman[9] and Neira and Payatakes[21] for the same problem.

When the amplitude of the wall oscillations is large, a recirculation zone starts to appear near the wall of the tube in the expansion region. Under these conditions the nine-node element becomes unstable in the description of the velocity field and the instabilities are propagated throughout the whole domain of integration. For example, let us consider the sinusoidal tube with wall profile

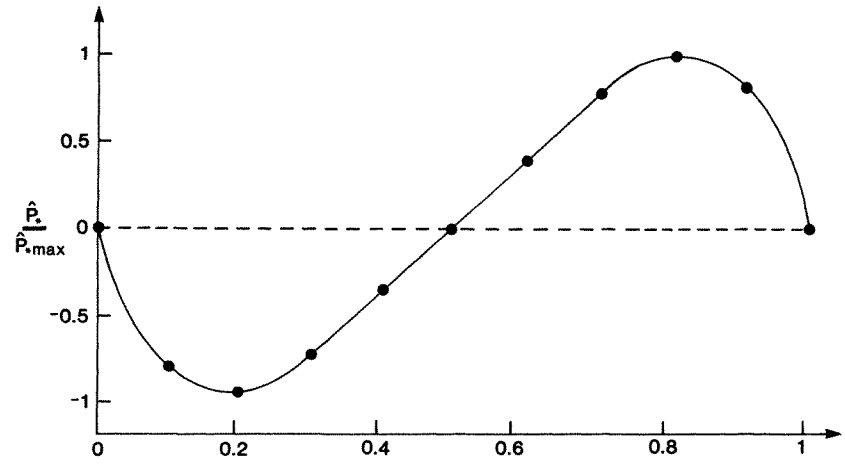

Figure 7. Periodic pressure field at $r = 0$. Wall profile described by equation (29)

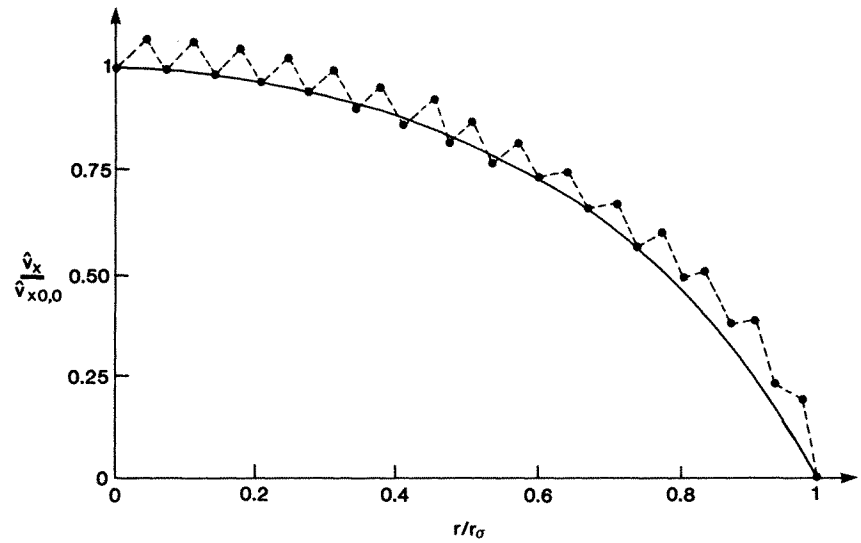

Figure 8. Axial velocity at $x = 0$. Wall profile described by equation (30)

given by

$$r_\sigma(x) = 3(1 - 0{\cdot}7 \cos 2\pi x). \tag{30}$$

Figures 8–10 show the velocity profiles obtained for both types of elements for a grid of 180 elements. The solid lines are, again, smooth lines through the eight-node element results and the dots are the nine-node element results. The dots have been joined by dashed lines for a better visualization of the oscillatory behaviour. The eight-node results shown were the same

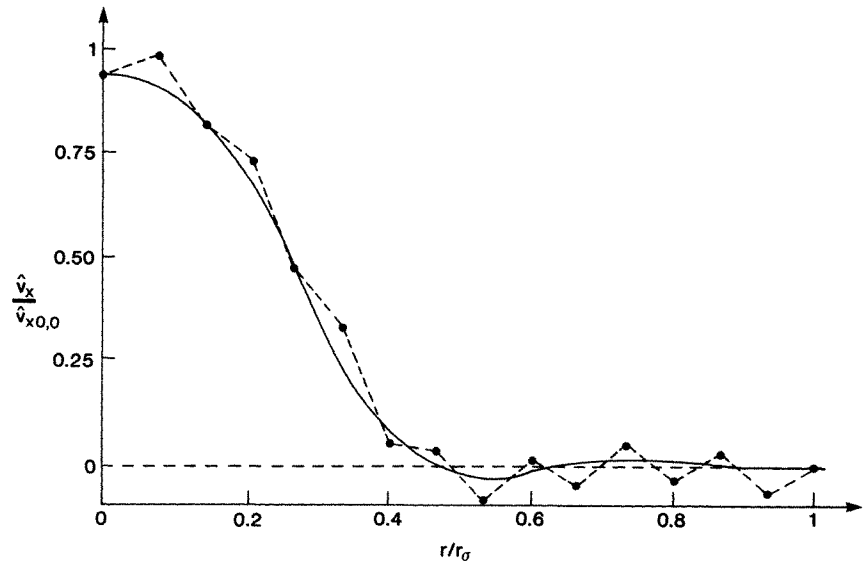

Figure 9. Axial velocity at $x = 0{\cdot}5$. Wall profile described by equation (30)

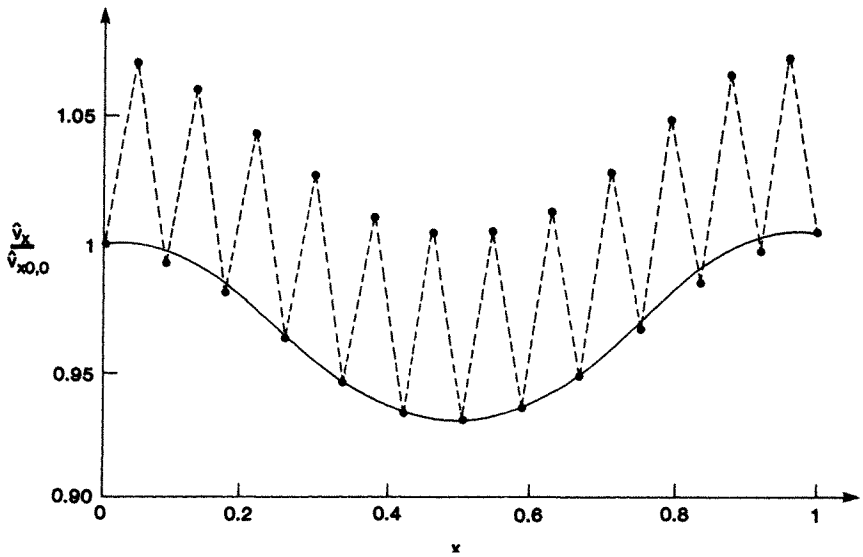

Figure 10. Axial velocity at $r = 0$. Wall profile described by equation (30)

as those obtained with a coarser grid of 60 elements, indicating that convergence has been achieved. The nine-node results kept oscillating with a period equal to the element size even for finer grids so that convergence was never achieved for this type of element. The magnitude of the oscillations is not very large but they are relatively important especially in representing variations of v_x with respect to x (Figure 10). Even though in the average both elements give very similar results, the instabilities of the nine-node element could lead to high errors if those results were used in other types of calculations such as the evaluation of dispersion coefficients.

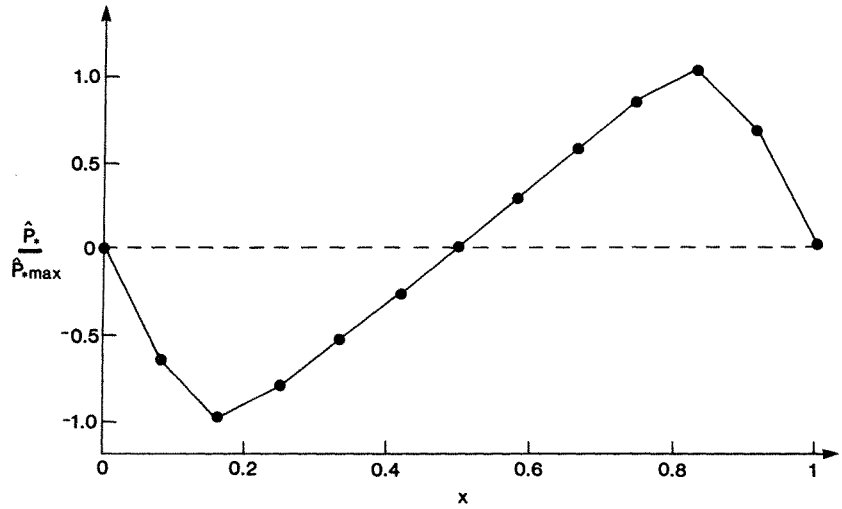

Figure 11. Periodic pressure field at $r = 0$. Wall profile described by equation (30)

Regarding the pressure field, we can observe (see Figure 11) that both elements give exactly the same results. Notice that the results obtained in the present work show a completely opposite behaviour to those obtained by Huyakorn *et al.*[7] in the case of flow through a sudden expansion. In our case the oscillations are exhibited by the nine-node element solution in the velocity field whereas in their case the oscillatory patterns were observed in the pressure field by the eight-node element solution. We should emphasize that the only qualitative differences between the two problems are the boundary conditions at entrances and exits.

As we pointed out before, the only difference between the eight- and nine-node element approximations is the presence of a fourth-order term (r^2x^2) in the approximating function of the Lagrangian nine-node scheme. It is possible then to speculate that this term has an important effect on the stability of the solution. The global effect seems to be the occurrence of a decoupling between vertex and mid-side and centre nodes in the nine-node elements: if we plot the velocity profiles by considering only vertex or mid-side and centre nodes, we obtain two different smooth curves. We have not found an explanation for this behaviour. Further studies are required to establish the cause and possible solutions for this problem.

CONCLUSIONS

A study of the performance of various finite element formulations in the solution of the flow problem through periodically constricted tubes was performed. It was found that the use of the continuity equation to reduce the viscous terms in the Stokes equations from the gradient of the stress tensor to the Laplacian of the velocity decreased the rate of convergence of the algorithm.

It was determined that the eight-node serendipity element is more adequate in this case than the nine-node Lagrangian element for tubes with large expansion zones. The nine-node element solution exhibited oscillatory velocity fields even for very fine grids whereas the eight-node element converged smoothly to the final solution. The accuracy in the prediction of the pressure field was the same for both types of elements.

The results obtained in the present work, when compared to previous results available in the literature, indicate that the boundary conditions play a crucial role in determining the performance

of certain types of finite elements. This fact calls for more extensive theoretical work in order to try to establish the causes of unstable patterns.

REFERENCES

1. B. Atkinson, C. C. Card and B. Irons, 'Applications of the finite element method to creeping flow problems', *Trans. Inst. Chem. Eng.*, **48**, 276 (1970).
2. J. T. Oden and L. C. Wellford, 'Analysis of flow of viscous fluids by the finite element method', *AIAA Journal*, **10**, 1590 (1972).
3. C. Taylor and P. Hood, 'A numerical solution of the Navier–Stokes equations using the finite element technique', *Computers and Fluids*, **1**, 73 (1973).
4. M. Olson and S. Tuann, 'Primitive variables versus stream function finite element solutions of the Navier–Stokes equations' in *Finite Elements in Fluids*, Volume 3, Wiley, Chichester, 1978.
5. R. L. Sani, P. M. Gresho, R. L. Lee and D. F. Griffiths, 'The cause and cure (?) of the spurious pressures generated by certain FEM solutions of the incompressible Navier–Stokes equations: part 1', *Int. J. Num. Meth. Fluids*, **1**, 17 (1981).
6. R. L. Sani, P. M. Gresho, R. L. Lee, D. F. Griffiths and M. Engelman, 'The cause and cure (?) of the spurious pressures generated by certain FEM solutions of the incompressible Navier–Stokes equations: part 2', *Int. J. Num. Meth. Fluids*, **1**, 171 (1981).
7. P. S. Huyakorn, C. Taylor, R. L. Lee and P. M. Gresho, 'A comparison of various mixed-interpolation finite elements in the velocity-pressure formulation of the Navier–Stokes equations', *Computers and Fluids*, **6**, 25 (1978).
8. M. A. Neira and A. C. Payatakes, 'Collocation solution of creeping Newtonian flow through periodically constricted tubes with piecewise-Continuous wall profile', *AIChE Journal*, **24**, 43 (1978).
9. P. Fedkiw and J. Newman, 'Mass transfer at high Péclet numbers for creeping flow in a packed bed reactor', *AIChE Journal*, **23**, 255 (1977).
10. J. A. Deiber and W. R. Schowalter, 'Flow through tubes with sinusoidal axial variations in diameter', *AIChE Journal*, **25**, 638 (1979).
11. J. C. F. Chow and K. Soda, 'Laminar flow in tubes with constriction', *The Physics of Fluids*, **15**, 1700 (1972).
12. A. E. Sáez, R. G. Carbonell and J. Levec, 'The hydrodynamics of trickling flow in packed beds, part I: conduct models', *AIChE Journal*, in press.
13. A. E. Sáez, 'Hydrodynamics and lateral thermal dispersion for gas–liquid concurrent flow in packed beds', *Ph.D. Dissertation*, University of California, Davis, 1984.
14. E. B. Becker, G. B. Carey and J. T. Oden, *Finite Elements. An Introduction*, Vol. I, Prentice-Hall, New Jersey, 1981.
15. L. R. Herrmann, 'Laplacian–isoparametric grid generation scheme', *J. Eng. Mech. Div., Proceedings of the ASCE*, **102**, 749 (1976).
16. J. M. Leone, P. M. Gresho, S. T. Chan and R. L. Lee, 'A note on the accuracy of Gauss–Legendre quadrature in the finite element method', *Int. J. Num. Meth. Eng.*, **14**, 769 (1979).
17. G. F. Carey and J. T. Oden, *Finite Elements. A Second Course*, Vol. II, Prentice-Hall, New Jersey, 1983.
18. P. Hood, 'Frontal solution program for unsymmetric matrices', *Int. J. Num. Meth. Eng.*, **10**, 379 (1976) and **11**, 1055 (1977).
19. R. L. Taylor, 'On completeness of shape functions for finite element analysis', *Int. J. Num. Meth. Eng.*, **4**, 17 (1972).
20. O. C. Zienkiewicz, B. M. Irons, J. G. Ergatoudis, A. Ahmad and F. C. Scott, 'Iso-Parametric and associate element families for two and three dimensional stress analysis' *in Finite Element Methods in Stress Analysis*, Tarpir Press, Norway, 1969.
21. M. A. Neira and A. C. Payatakes, 'Collocation solution of creeping Newtonian flow through sinusoidal tubes', *AIChE Journal*, **25**, 725 (1979).